





Low loss double cladding nested hollow core antiresonant fiber

KUMARY SUMI RANI SHAHA,^{1,3} ABDUL KHALEQUE,^{1,4}  AND MD IMRAN HASAN² 

¹Department of Electrical & Electronic Engineering, Rajshahi University of Engineering & Technology, Rajshahi-6204, Bangladesh

²Optical Sciences Group, Research School of Physics, The Australian National University, Acton ACT 2601, Australia

³sumi.ss.bd@gmail.com

⁴abdul.khaleque.eee@gmail.com

Abstract: A double cladding nested antiresonant hollow core fiber is reported in this article. We demonstrated that the addition of nested elements in the second cladding ring and the proper optimization of structural parameters lead to the loss reduction by more than five orders. The numerical simulation exhibits a loss of less than ~ 0.1 dB/km over the O, E, S, C, L telecom bands, with the minimum loss of 0.001 dB/km at 1.40 μm wavelength with a fiber core diameter of 33 μm . The fiber also shows a better performance in terms of bending loss as well as single modeness, and may have effective applications in a telecommunication system.

© 2020 Optical Society of America under the terms of the [OSA Open Access Publishing Agreement](#)

1. Introduction

Hollow core fibers (HCFs) are such a fiber which confine light in the central hollow region, can be filled with air or gas or liquid [1]. Recently, a large amount of research has been carried out on HCFs due to their enchanting features along with reduced loss, low group velocity dispersion (GVD), and high optical damaged threshold [2–6] and so on. The above-mentioned features lead HCFs in many applications including optical communication [7,8], high power pulse delivery [9], gas-based light source [10,11], and supercontinuum generation [3,12]. Based on guiding property there are two main types of HCFs: hollow core photonic bandgap fibers (HC-PBGFs) and hollow core antiresonant fibers (HC-ARFs). HC-PBGFs provide the opportunity to obtain low transmission loss but have limited bandwidth along with intense GVD [13–15]. On the other hand, HC-ARFs perform better than the HC-PBGFs in terms of wide bandwidth but show a quite high loss as well as high bend sensitivity [7,16]. In addition, surface scattering loss (SSL) limiting the achievement of PBGFs [15] that can be suppressed significantly in HC-ARFs [16]. Due to the recent progress and enough research scope, the later type gets much more interest in the current work.

The guiding aspect, which is inhibited coupling [16–18], of HC-ARFs largely relies on the cladding structure such as antiresonant tubes, which create antiresonant reflection enclosing the core. To be more specific, the cladding elements are made in such a way that induces a massive index mismatch between core and cladding modes, hence, prevents the light leaking from the core and leads to reduce confinement loss [4] significantly. A large diversity of HC-ARFs, based on cladding geometry [7,8,16–23] are available. A small gap between the adjacent cladding tubes consequently alleviates the loss that appears due to the resonance of nodes [16]. In recent years, it is reported that by adjoining an array of a smaller nested tube in the HC-ARFs the light leakage loss can be substantially reduced because of the supplementing antiresonant reflection [8,16,17]. For example, Bradley and colleagues [8] reported a six tubes nested fiber and demonstrated a loss of 1.3 dB/km at 1.45 μm wavelength. Few more numerical reports are also proposed by adding an extra layer of antiresonant tubes in HC-ARFs [24–26], thus leads to an extra degree of freedom

which is responsible for monitoring light leakage. Recently, Wang *et al.* [24] demonstrated a double ring negative curvature fiber (DR-NCF) and analyzed the effect of admitting the second ring of cladding elements for high-power laser application. Therefore, it is highly demanded to achieve the best characteristics of both PBGFs and ARFs on a hollow core platform and can meet the requirements (low loss, wide bandwidth, bend insensitive, and single modeness etc.) of the current optical communication system.

In this work, we proposed a fiber that can perform well with very low loss over broad range as well as better bending loss and high single mode characteristics. The proposed fiber shows a record low loss of 0.001 dB/km at the wavelength of 1.40 μm while maintaining the low loss of $< \sim 0.1$ dB/km over the broad bandwidth of 320 nm (1.28 μm to 1.6 μm). The additional inverse curvatures associated with the core boundary, supplements the antiresonant reflection and leads to better confinement of light in the core. It also exhibits better bending loss of ~ 0.01 dB/km for the bend radius of 8 cm at 1.45 μm wavelength along with an effective single mode operation with the highest HOMER of 10000. The proposed double cladding nested antiresonant hollow core fiber (DCN-AR-HCF) illustrates the best performance to the best of our knowledge, may have potential applications in the optical communication system.

2. Fiber design

Figure 1 illustrates a cross-section of the proposed DCN-AR-HC fiber, which consist of two rings. The first ring has five antiresonant tubes whereas the second ring has ten antiresonant tubes. In the proposed structure an additional nested element has been added in the antiresonant tube of the second ring, which increases the number of negative curvatures in the cladding. This arrangement improved the light reflection at the interface and hence, the confinement loss reduced significantly. Note that the cladding tubes of the first ring are evenly spaced and simultaneously they are placed by the same azimuthal angle with the second ring antiresonant tubes. The designed parameters are optimized to get the lowest confinement loss over the telecommunication windows, i.e., 1260

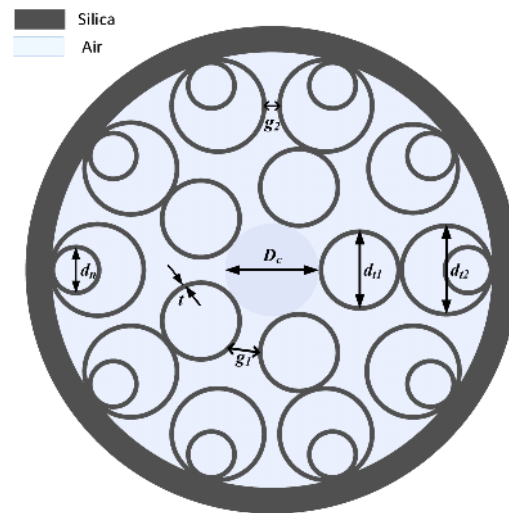


Fig. 1. Idealized cross-sectional of proposed DCN-AR-HC fiber. Here, D_c and t represent the hollow core diameter and the glass-web thickness respectively. In the first ring, d_{t1} and g_1 are the diameter of the antiresonant tubes and perimeter gap between two tubes respectively. Similarly, d_{t2} and g_2 denote the diameter of the antiresonant tubes and the perimeter gap, respectively, for the second ring cladding. The diameter of the nested tube is $d_n = d_{t2}/2$.

nm to 1625 nm. The structure basically proposed a design of a bend insensitive and single-mode HC-ARF to satisfy the loss requirements of existing fiber used for the communication system.

In this work, fiber core diameter $D_c = 33 \mu\text{m}$ and glass-web thickness $t = 580 \text{ nm}$ will remain fixed as presented above. In Fig. 1, n_1 and d_{r1} denote the number of antiresonant tubes and the corresponding tube diameter that installed in the first ring. Similarly, n_2 and d_{r2} are the number of antiresonant tubes and the corresponding tube diameter which are considered in the second ring. The second ring has a set of nested elements, where the diameter d_n is considered half of the d_{r2} ($d_n = d_{r2}/2$). The perimeter gap between two antiresonant tubes in the first ring is subjected by the proper choice of D_c , t , n_1 , and d_{r1} which are considered by the expression: $D_c = (D_1 + 2t + g) / \sin(\pi/n) - (D_1 + 2t)$ [4]. The inner nested tube penetrates the outer tube by $t/2$ and the antiresonant tubes of the second ring infused by $t/2$ into the outer jacket in order to achieve the numerical simulation closer to the practical case.

3. Results and discussion

In order to perform the numerical simulations, a finite element method has been considered. To see the accuracy of our results, few related structures [4,24,25], available in the literature, are simulated first and found good agreement. In the next step, we have performed a convergence test on our proposed structure to optimize the mesh size and the boundary layer thickness according to the literature [16]. To do that confinement loss (CL) is plotted with respect to perfectly matched layer (PML) thickness and the mesh size parameter (p). Confinement loss is the vital loss mechanism of fiber, which arises because of the leaky nature of light confinement in the core and is calculated by the following expression [25,27] as

$$\text{CL} = \frac{40\pi \times \text{Im}(n_{\text{eff}})}{[\ln(10) \times \lambda]} \times 10^6 \text{ (dB/m)} \quad (1)$$

where $\text{Im}(n_{\text{eff}})$ and λ represent the imaginary part of the fundamental mode (FM) mode effective refractive index and the wavelength, respectively.

As an example, Figs. 2(a) and 2(b) represent the CL versus PML thickness and CL versus p , respectively, where p is the integer. These convergences have a trial done at $1.4 \mu\text{m}$ with the user-defined mesh sizes of $\lambda/6p$ for silica and $\lambda/4p$ for the air. From these numerical simulations, it is noticed that PML becomes stable for layer thickness beyond $1.0 \mu\text{m}$ as shown in Fig. 2(a) and finally we used around $10 \mu\text{m}$ PML thickness for the numerical study of the proposed fiber. At the same time, the maximum mesh size of $\lambda/4$ and $\lambda/6$ are chosen for glass and air region, respectively, since the simulation is stable after $p = 1$ as shown in Fig. 2(b).

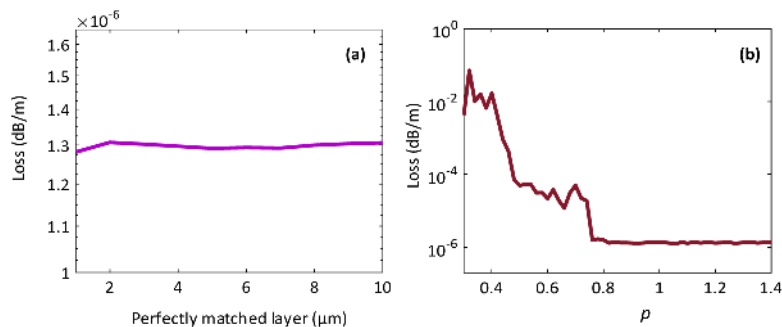


Fig. 2. The convergence analysis of the proposed structure for (a) the PML thickness, and (b) the mesh size parameter (p) where $\lambda/4p$ and $\lambda/6p$ used for air and silica, respectively, at $1.4 \mu\text{m}$.

HC-ARFs have a narrow bandwidth region, in which, the hollow core mode strongly coupled with the glassy cladding modes that create resonance and suffering with an unpleasant loss performance. The resonance condition can be expressed as follows [4]

$$\lambda = \frac{2t\sqrt{n_g^2 - n_a^2}}{w} \quad (2)$$

where t is the glass-web thickness, n_g and n_a , represent the refractive indices of silica, and air material respectively, λ is the operating wavelength, and w is the positive integer number: $w = 1, 2, 3, \dots$, that represents the transmission window. Since the $t = 580$ nm in the work, the first resonance region around $1.21 \mu\text{m}$ wavelength is considered according to the above resonance condition. On the other hand, there is a low loss region for broad bandwidth, where the core mode has an antiresonant effect with the cladding modes that form inhibited coupling among them.

In the proposed structure, there are four controlling functions (n_1, d_{t1}, n_2, d_{t2}), and by keeping $n_1=5$ and $n_2=10$ fixed; we optimized the diameters of those two cladding rings by the function of d_{t1}/D_c and d_{t2}/D_c , respectively. Figures 3(a) and 3(b) represent the confinement loss of fundamental mode (FM) as a function of d_{t1}/D_c and d_{t2}/D_c respectively. First of all, we optimized the first ring antiresonant tubes diameter (d_{t1}) by the normalized function of d_{t1}/D_c . It is seen from Fig. 3(a) that the confinement loss decreases gradually as d_{t1}/D_c decreases from 1.1 and the loss remains almost flat over $0.65 < d_{t1}/D_c < 0.85$ range. By optimizing d_{t1}/D_c function very delicately, we found the minimum loss at around $d_{t1}/D_c = 0.7$ that is appreciable for practical use i.e. fabrication tolerance. After fixing $d_{t1}/D_c = 0.7$ to its optimum value, we introduce the antiresonant tubes inside the second ring and started to optimize the diameter of the tubes as a function of d_{t2}/D_c . It is noticed from Fig. 3(b) that the FM loss decreases as d_{t2}/D_c decreases starting from 1.1 and maintains the loss curve almost flat within the range of around $0.65 < d_{t2}/D_c < 0.9$. For fabrication simplicity, we have used $d_{t2}/D_c = 0.85$ as optimum value for further the analysis. Since the loss does not vary much with the variation of nested tube parameter within the above range [19], the diameter of nested tube is chosen as $d_n = d_{t2}/2$.

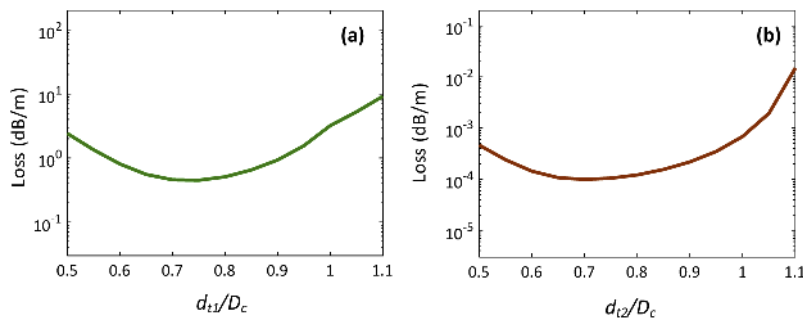


Fig. 3. The confinement loss with respect to (a) d_{t1}/D_c for the first ring antiresonant tubes, and (b) d_{t2}/D_c for the second ring antiresonant tubes, at the wavelength of $1.4 \mu\text{m}$.

3.1. Confinement loss

Up to date, numerous works are studied which are considered with different cladding structures [4,7,16,18], along with the additional layer of cladding structure [24–26]. Likewise, in the previous study, to avoid the extra resonator the proposed structure is retaining nodeless. In addition to this, nested elements are added in the second ring, which can supplement the antiresonant reflection and can confine the light strongly in the core, therefore, the leakage loss

will be reduced significantly. In Fig. 4, the effects of the adding second ring cladding is analyzed first over single cladding geometry and tried to achieve a best structure which can fulfill our first expected goals (i.e. lowest loss). After that, the effects of nesting in second ring cladding is observed (blue color curve with diamond marker) and found best performance to choose as proposed structure. All three structures are considered based on the optimized structural parameters as $D_c = 33 \mu\text{m}$, $t = 580 \text{ nm}$, $d_{11}/D_c = 0.7$ (for SR-NCF), $d_{12}/D_c = 0.85$ (for DC-NCF), and $d_n = d_{12}/2$ (for nesting in proposed fiber).

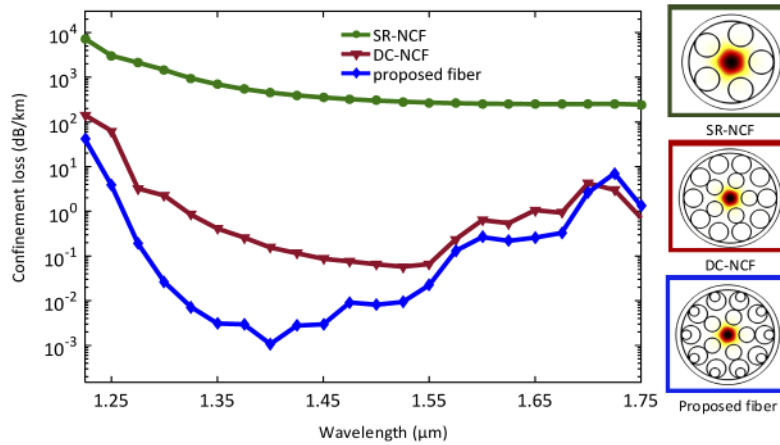


Fig. 4. The process of achieving lowest confinement loss spectra for our fiber. The structure is modified from a single ring fiber (SR-NCF) to double cladding fiber (DC-NCF), and finally the proposed double cladding nested antiresonant hollow core fiber (DCN-AR-HCF). The used fiber parameters are $D_c = 33 \mu\text{m}$, $t = 580 \text{ nm}$, $d_{11}/D_c = 0.7$, $d_{12}/D_c = 0.85$, and $d_n = d_{12}/2$. The right-hand side frame depicts the corresponding field profiles of the structures and line color of loss curve correlates with the frame color of corresponding structures.

It is observed from Fig. 4 that the loss, within the band of interest, is higher for single ring fiber (curve with circle marker) and then decreased remarkably due to the addition of second cladding ring (curve with triangle marker). Hence, the second cladding ring has a significant impact on loss performance as it increases the negative curvature as well as enlarges antiresonant reflection, therefore reduces the magnitude of loss up to around four orders. Furthermore, introducing a set of nested elements within tubes of second ring cladding provide the least number of nodes which results in more antiresonant reflection; hence, the fiber offers the best performance (loss reduced by five order of magnitude).

In the next step, the loss performance of the proposed structure is compared with the recent related three structures from the literature [19,24,26] which are five tubes based single ring nested antiresonant nodeless fiber (NANF), a two-ring split cladding fiber (2SCF), and a double ring NCF (DR-NCF). Due to the fair assessment, all the considered structures have same core diameter of $D_c = 33 \mu\text{m}$ as well as same glass-web thickness of $t = 580 \text{ nm}$ while other dimensions are optimized delicately along with the same spectral region of $1.225 \mu\text{m}$ to $1.75 \mu\text{m}$. It is noticeable from Fig. 5 that the loss of proposed fiber can be reduced up to nearly three orders with comparing to 2SCF and NANF. The reasons for the loss reduction is already discussed before in Fig. 4. It can be mentioned that the proposed fiber performs better than the other studied structures as well: the lowest loss accomplished at $1.4 \mu\text{m}$ wavelength that is 0.001 dB/km and remains less than $\sim 0.1 \text{ dB/km}$ over the broad range of 320 nm . Due to the existence of the extra resonator or extra joining point, the loss increases at higher wavelengths region as agreed with [24]. Therefore, it is concluded from Fig. 4 that the loss magnitude is reduced by more than five orders compared to single cladding geometry (SR-NCF) by simply introducing the nested second

ring of antiresonant tubes with proper optimization of designed parameters and the findings should be useful in telecommunication application.

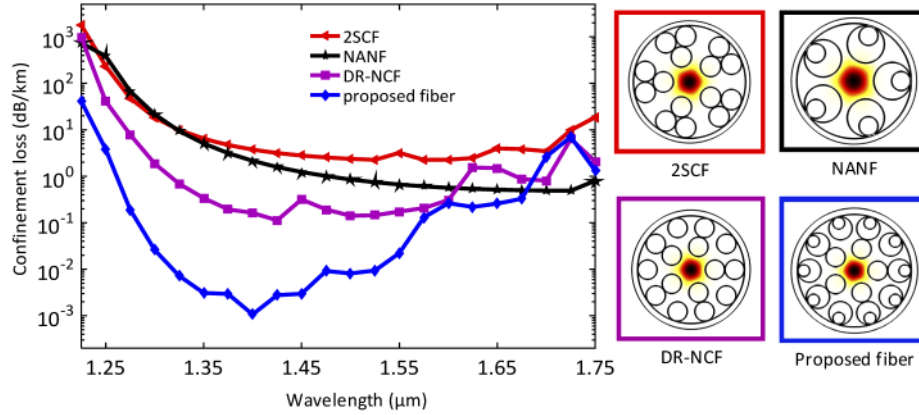


Fig. 5. The comparative loss spectra among 2SCF, NANF, DR-NCF, and the proposed fiber. All structures used $D_c = 33 \mu\text{m}$ and $t = 580 \text{ nm}$. In addition, $d_i/D_c = 0.621$ (for all tubes in 2SCF); $d_i/D_c = 1.05$ (for outer tubes as well as half of its inner tubes in the NANF); $d_{i1}/D_c = 0.663$, and $d_{i2}/D_c = 0.667$ (for DR-NCF). The proposed structure used $d_{i1}/D_c = 0.7$, and $d_{i2}/D_c = 0.85$, and $d_n = d_{i2}/2$. The right-hand side frame depicts the corresponding field profiles of the structures and line color of loss curve correlates with the frame color of corresponding structures.

3.2. Bending loss

Bending loss is another significant issue in practical application and can't be avoided. In this regard, the proposed fiber design tried to achieve bend insensitive performance as much as possible so that the light can be confined with reduced loss at the point of around corner. The bending loss occur in core modes of HC-ARFs due to the coupling between core and tube modes. It is reported that the structure which admitted with additional ring of cladding element can assist to improve the bend robustness [16]. Therefore, to calculate the bending loss of the proposed fiber, we imply a conformal transformation for modifying the refractive index (n') of the bended fiber with an equivalent to the straight fiber [28] as

$$n' = n_m \cdot e^{\left(\frac{x}{R_b}\right)} \sim n_m * \left(1 + \frac{x}{R_b}\right) \quad (3)$$

where n' is the conformed refractive index, n_m is the refractive index of the material of the proposed fiber under no strain or a straight fiber, R_b represents the curvature radius, and x denotes the location of direction of bending from the fiber center as we assume the bending direction along with the x -axis.

Figure 6 illustrates the bending loss as a function of bend radius for the five tube SR-NCF, NANF, DC-NCF, and the proposed fiber (DCN-AR-HCF) at a guidance of $1.5 \mu\text{m}$ wavelength. The dimensions of $D_c = 33 \mu\text{m}$, and $t = 580 \text{ nm}$ are same for above four structures but other parameters are considered as discussed in Figs. 4 and 5. It has observed from Fig. 6 that the bending loss monotonically decreases with the increase of the bend radius. Among the fundamental mode (FM) bending loss curves of those fibers, the proposed DCN-AR-HC fiber reveals the lower loss at the bend radii of greater than of 5 cm , where the bending loss remains less than 0.4 dB/km . The severe peak of bending loss is observed at around 4 cm bend radius due to anti-crossing effect between the core mode and cladding mode as shown in Fig. 6 (right). The

lowest bending loss of ~ 0.01 dB/km is found at the bend radius of around 8 cm as can be seen in Fig. 6. In fact, with compare to DC-NCF and NANF fibers, the loss is reduced by around two orders of magnitude.

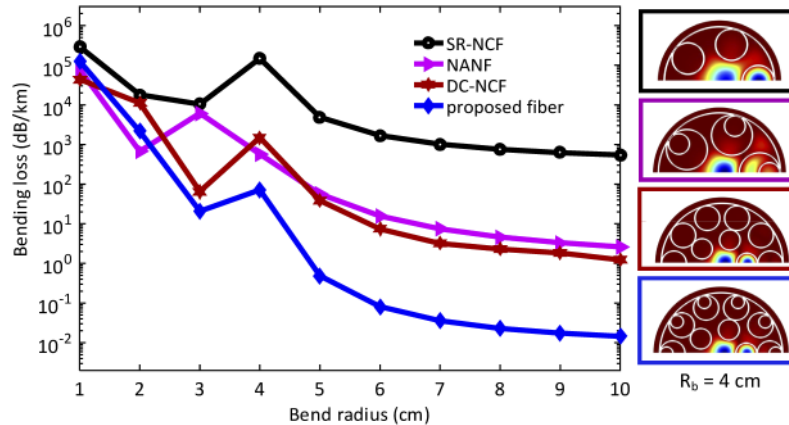


Fig. 6. The bending loss versus bend radius for four geometries (SR-NCF, NANF, DC-NCF, and DCN-AR-HCF) at $1.5 \mu\text{m}$. Parameters are chosen as discussed in Figs. 4 and 5. At $R_b = 4$ cm, the corresponding field profiles are in the right side. The line color correlates with frame color.

Another bending radius of 8 cm is considered here to see the bending loss performance as a function of wavelength for the four structures (top of the Fig. 7(a)). It is noticed from Fig. 7(a) that the proposed fiber gives least loss spectra compared to all studied structures: the lowest loss of ~ 0.01 dB/km is found at $1.45 \mu\text{m}$ wavelength and loss remains below 1 dB/km from around $1.35 \mu\text{m}$ to $1.61 \mu\text{m}$ of wavelength. It is also seen that the SR-NCF exhibits the highest loss among the studied structures. On the other hand, the bending loss spectra is calculated for the proposed fiber at different bend radii (Fig. 7(b)) and it is observed that loss magnitude decreases with the increase of bend radius which is expected and still the bandwidth remains wide. In summary, the proposed fiber can maintain a bending loss of less than 1 dB/km over 300 nm of bandwidth for the bend radius of 8 cm as can be seen in Figs. 7(a) and 7(b).

3.3. Single mode performance

In this section, we inspected the single mode performance of our proposed DCN-AR-HCF because fiber may have higher order modes (HOMs). If the HOMs losses are substantially high compared to the FM loss, then the fiber can be operated adequately as a single mode fiber. In this work, we tried to calculate higher order mode extinction ratio (HOMER) which can point out the light leakage loss of HOMs with concerning to the leakage loss of FM. We investigate the loss of first six core modes (fundamental and HOMs) namely HE_{11} , TE_{01} , TM_{01} , HE_{21} , EH_{11} , and HE_{31} mode.

Figure 8(a) depicts the confinement loss of first four core modes as a function of the wavelength. The loss of FM like HE_{11} attains its minimum loss at $1.40 \mu\text{m}$, on the contrary, the loss of the HOMs (TE_{01} , TM_{01} , HE_{21} , EH_{11} , and HE_{31}) reaches its minimum around $1.50 \mu\text{m}$ and shows a small loss peak at $1.45 \mu\text{m}$. It is known that the high loss value of HOMs can be achieved on account of the strong coupling between the cladding modes and higher order core modes [16]. Similarly, in this work, the large loss value of HOMs is attained by designing proper antiresonant cladding geometry consisting of nested second cladding ring which leads to couple higher order core modes with the cladding modes. The aim of every work is to maintain the HOMER at least >10 , over a broadband, to maintain an acceptable single mode performance [24] and the

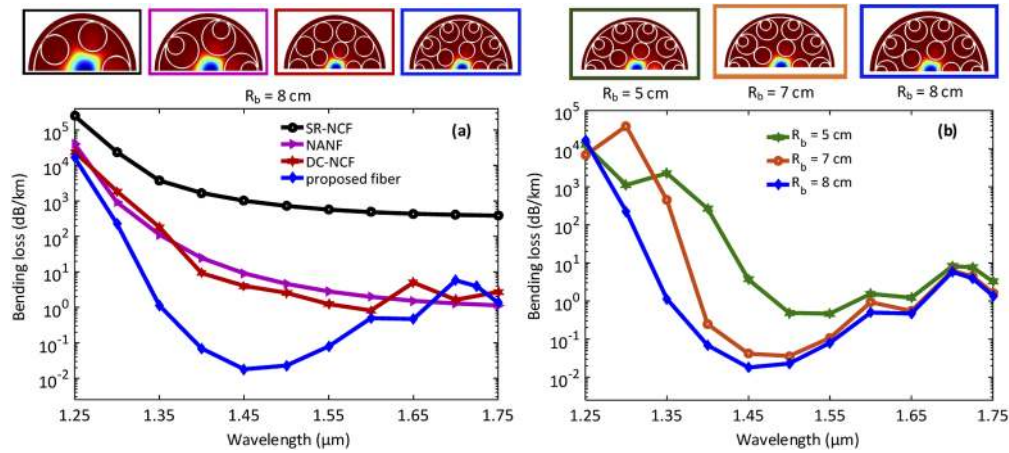


Fig. 7. The comparative bending loss performance over wavelength of interest (a) for different structures (same as shown in Fig. 6) at the bend radius of 8 cm, and (b) for different bend radii ($R_b = 5, 7, 8$ cm) of proposed structure. The corresponding FM field profiles are given in upper panel, and the displayed line color on the plot exerted the color of frame.

proposed work is also tried to achieve HOMER as high as possible over a wide wavelength range. The highest HOMER of about 10000 is found around at 1.45 μm and the value remains greater than 100 over the both communication windows as can be seen in Fig. 8(b).

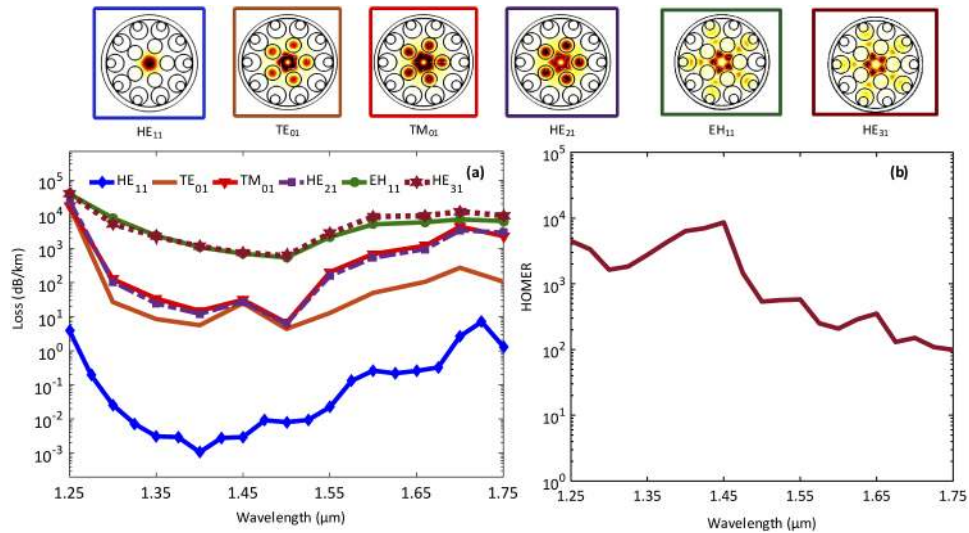


Fig. 8. (a) The loss performance of proposed fiber (loss of fundamental and HOMs) as a function of wavelength, and (b) HOMER versus wavelength. Here, TE_{01} shows the lowest loss among all HOMs. The top panel exhibits the modal content for FM and three HOMs. The line colors inside the plot correspond to the frame color.

Table 1 summarizes the all performance parameters of the proposed fiber and few recent related fibers available in the literature. The first one [7] is a conjoined tube HC-ARF that used five conjoined tubes with a core diameter of 30.5 μm and showed the optical loss of 2 dB/km at 1.512 μm . It also reports a loss of 16 dB/km over 335 nm bandwidth, and 1 dB/km bending loss for 10 cm bend radius. In addition, literature [8] reported a six tubes nested single ring fiber and

shows a loss of 1.3 dB/km at 1.45 μm wavelength, and maintains a loss of <2 dB/km over 90 nm bandwidth. Moreover, Debord and co-workers [20] reported a HC-ARF which is made by single ring of eight non-touching antiresonant tubes as cladding elements and mentioned a loss of 7.7 dB/km at the wavelength of 750 nm with a bending loss of 0.03 dB/turn for 15 cm bend radius. In literature [25], Chen and colleagues proposed a double negative curvature fiber having six large tubes and six small tubes. They are arranged in a staggered pattern showing a propagation loss less than 0.1 dB/km around 1.35 μm .

Table 1. Performance comparison of the proposed device with the recent related existing literatures.

Ref. (Year)	Transmission window	Minimum attenuation (dB/km)	Bending loss (dB/km)	Dc (μm)
[7] (2018)	16 dB/km for 335 nm	2 dB/km at 1.512 μm	<1 dB/km for R = 10 cm	30.5
[8] 2019	2 dB/km for 90 nm	1.3 dB/km at 1.45 μm	<0.1 dB/km	31
[20] (2019)	10–20 dB/km for 600 nm	7.7 dB/km at 750 nm	0.03 dB/turn for R = 15 cm	27.5 to 37
[25] (2019)	<1 dB/km for 400 nm	0.25 dB/km at 1.35 μm	Not reported	40
Prop. HC-ARF (2020)	<0.1 dB/km for 320 nm	0.001 dB/km at 1.4 μm	~ 0.01 dB/km for R = 8 cm	33

Concerning the above comparative analysis, the proposed fiber reports the best performance: the lowest loss of 0.001 dB/km is achieved at the wavelength of 1.4 μm while loss remained less than ~ 0.1 dB/km over a wide bandwidth of 320 nm. Moreover, the fiber exhibits low bending loss (around 0.01 dB/km at 8 cm bend radius) and better single mode performance compared to the available literature as can be observed in Table 1. There are more fibers (not listed in Table 1) to achieve ultra-low transmission loss and better single mode performance e.g. double ring cladding tubes [24,26], hybrid cladding tubes [22], nested cladding tubes [16,17] but our proposed DCN-AR-HC fiber shows best performance due to its low loss, bend insensitivity, and better single mode performance over telecommunication bandwidth.

4. Fabrication feasibility

On account of real-world application, it is essential to evaluate the susceptibility of structural parameter variation on the fiber performance so that the final geometry can maintain the expected outputs after fabrication. In this work, the contact point between the adjacent tubes in the first and second ring contain the edge thickness of $2t$ due to the mass defense and similar edge thickness also observed in some negative curvature fibers [18,24].

The percentage of fabrication error is investigated by considering the length of the edge thickness as a fraction of the periphery of the first ring tube. The fabrication tolerance is introduced on account of ideal edge thickness length with the increment of 4%, 6%, and 10% of edge thickness length as shown on the right side of Fig. 9. The impact on loss is observed in Fig. 9 with concerning the fabrication errors, mainly occurred due to interfusion of first ring tube and second ring tube that increase the edge layer thickness length. In Fig. 9, the worst case scenario is observed around the lowest loss portion compared to the other considered wavelength regions: the confinement loss increased by an order of magnitude, at the wavelength of 1.4 μm due to 6% fabrication error. With the presence of above shortcomings, the loss of the proposed fiber is still notably lower than that of the SR-NCF, NANF, DR-NCF, and 2SCF that can be seen in Figs. 4 and 5.

Moreover, it is relevant and important to demonstrate the angle of robustness between the fiber transversal axis and the contacting point (between the second ring inner nested tubes and outer tubes of cladding elements). Following the literature [17], we consider an identical shift of nested tube to represents the imperfection that offer an indication of fiber tolerance. For this work, φ

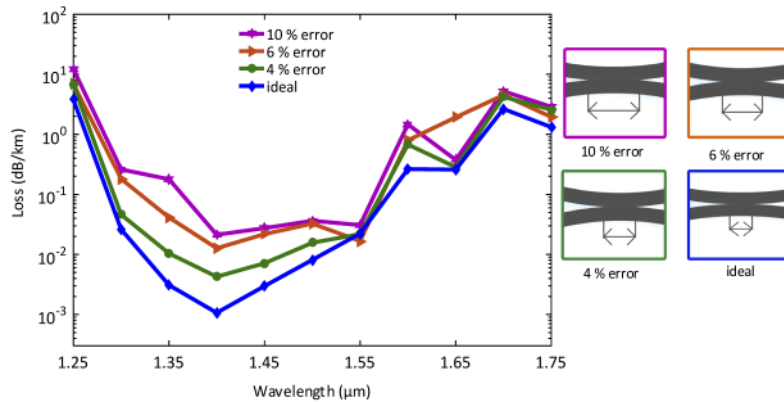


Fig. 9. The comparative loss curves of the ideal proposed fiber with the induced fabrication tolerance of 4%, 6%, and 10%. The percentage of fabrication tolerance of edge thickness is defined by the penetration of two-layer thickness. The right-side panel represents the edge thickness length of ideal fiber with the fabrication tolerance. The color of frame (right side) is used according to the line color in the plot.

denotes the identical shift of nested tube, and various fiber geometries are shown in Fig. 10 (right side panel), where φ varies from 0° to 140° for all nested tubes. Figure 10 represents the confinement loss as a function of φ at $1.5 \mu\text{m}$ wavelength. It is seen from Fig. 10 that the confinement loss remains steady when the angle (φ) varies from 0° to 110° , and then starts to increase significantly as φ increases beyond 110° . This happened due to movement of contact point of nested and second ring tubes toward the core, which increases the coupling between core and cladding modes [17]. Therefore, it is concluded that 110° shift can be tolerable to preform fabrication scheme of the proposed fiber. These numerical analysis reveals that a good level of fabrication flexibilities are allowed during preform of stacking preparation of this fiber type.

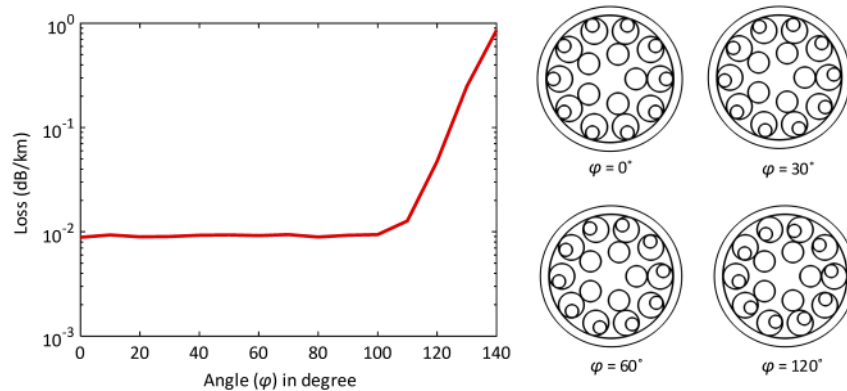


Fig. 10. The loss performance as a function of angle (φ) at $1.5 \mu\text{m}$ wavelength, where φ represents the angle between the fiber transversal axis and the contact point of nested and second ring tubes. The right side panel represents structures at different angle (φ).

In addition, it is necessary to reveal the influence of the displacement at the junction of first and second ring tubes due to the practical importance of fabrication. We consider a uniform shift of the junction of the first and second ring tubes to illustrate the imperfection that demonstrates the fiber tolerance. For this task, δ denotes the identical displacement of the junction, and some

fiber geometries are shown in Fig. 11 (right side panel), where δ varies from 0° to 22° for all junctions of the first and second ring tubes. Confinement loss is calculated as a function of δ at the wavelength of $1.50 \mu\text{m}$ as shown in Fig. 11. It is noticed from Fig. 11 that the confinement loss remains low and stable when the angle (δ) varies from 0° to 20° , and then starts to increase significantly as δ increases beyond 20° . This is happening due to the movement of first ring tubes toward the adjacent second ring tubes, that creates a node between them which is responsible for occurring resonance [16]. Therefore, it is concluded that the proposed fiber can well to tolerate 20° shift at the junction of the first and the second ring tubes during fabrication.

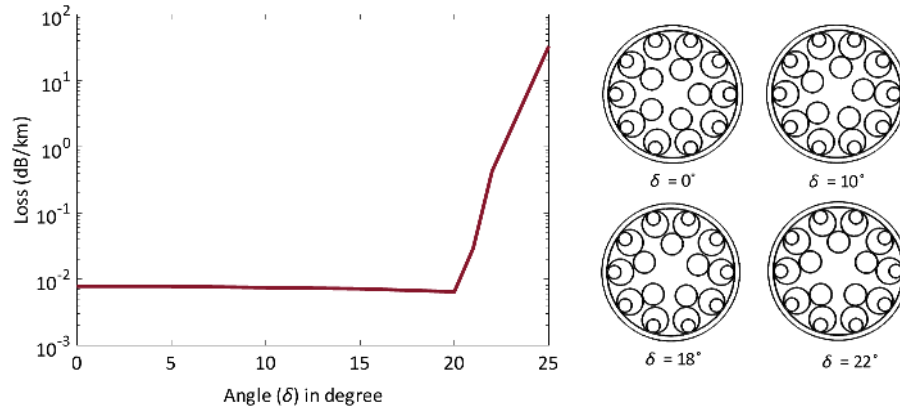


Fig. 11. The loss performance as a function of the junction displacement angle (δ) between first and second ring tubes at the wavelength of $1.50 \mu\text{m}$. The right panel depicts the structures at different displacement angle (δ).

There are few techniques available to fabricate HCFs. For example, stack and draw technique used in the fabrication of a HC-PBGF as the first prototype [1]. Other HCFs geometries have been fabricated by using comprehensive quick techniques such as stack and draw [14,20], extrusion [29], and 3D printing [30]. Besides, the 2SCF having three cladding rings used conventional stack-and-draw technique for its fabrication scheme [26]. In addition, stack-and-draw technique is used to fabricate negative curvature fiber with ice cream cone shape cladding elements [18], nested HC-ARFs [8,17], and conjoined tube HCFs [7]. Based on the above analysis, it is hoped that the proposed fiber should be feasible to fabricate by employing stack-and-draw technique.

5. Conclusion

We proposed and analyzed a DCN-AR-HC fiber, with the help finite element method, and claimed that the proposed work outperforms compared to the recently reported DR-NCF, NANF, and CTF. The contribution of nesting in second cladding ring leads to the achieved performance: the confinement loss is reduced by five order of magnitude. The fiber also shows low bending loss and high single mode characteristics over a broad band covering both well-known communication windows. Utterly, we obtained the lowest FM loss of 0.001 dB/km at $1.4 \mu\text{m}$ wavelength while it enduring less than $\sim 0.1 \text{ dB/km}$ loss over telecom bands, a bending loss of $\sim 0.01 \text{ dB/km}$ at 8 cm of bend radius, and a better single mode behavior (highest HOMER = 10000) of the fiber. Moreover, the fabrication tolerance for the proposed fiber has been studied and we believe that these numerical analyses administer an excellence guideline for its experimental realization. Therefore, the reported record low loss performances over broadband by the proposed DCN-AR-HCF can be attractive in the communication system.

Acknowledgments

The authors acknowledged the assistance provided by the Department of EEE of Rajshahi University of Engineering & Technology (RUET), Bangladesh. We also acknowledge the Research & Extension office of RUET for their support (DRE/7/RUET/489(31)/PRO/2020-21/09).

Disclosures

The authors declare no conflicts of interest.

References

1. R. F. Cregan, B. J. Mangan, J. C. Knight, T. A. Birks, P. S. Russell, P. J. Roberts, and D. C. Allan, "Single mode photonic band gap guidance of light in air," *Science* **285**(5433), 1537–1539 (1999).
2. F. Benabid, J. C. Knight, G. Antonopoulos, and P. S. J. Russell, "Stimulated Raman Scattering in Hydrogen Filled Hollow-Core Photonic Crystal Fiber," *Science* **298**(5592), 399–402 (2002).
3. P. S. J. Russell, P. Hölzer, W. Chang, A. Abdolvand, and J. C. Travers, "Hollow-core photonic crystal fibres for gas-based nonlinear optics," *Nat. Photonics* **8**(4), 278–286 (2014).
4. C. Wei, R. Joseph Weiblen, C. R. Menyuk, and J. Hu, "Negative curvature fibers," *Adv. Opt. Photonics* **9**(3), 504–561 (2017).
5. A. D. Pryamikov, A. S. Biriukov, A. F. Kosolapov, V. G. Plotnichenko, S. L. Semjonov, and E. M. Dianov, "Demonstration of a waveguide regime for a silica hollow-core microstructured optical fiber with a negative curvature of the core boundary in the spectral region $> 3.5 \mu\text{m}$," *Opt. Express* **19**(2), 1441–1448 (2011).
6. F. Couny, F. Benabid, P. J. Roberts, P. S. Light, and M. G. Raymer, "Generation and Photonic Guidance of Multi-Octave Optical-Frequency Combs," *Science* **318**(5853), 1118–1121 (2007).
7. S. F. Gao, Y. Y. Wang, W. Ding, D. L. Jiang, S. Gu, X. Zhang, and P. Wang, "Hollow-core conjoined-tube negative-curvature fibre with ultralow loss," *Nat. Commun.* **9**(1), 2828 (2018).
8. T. D. Bradley, J. R. Hayes, Y. Chen, G. T. Jasion, S. R. Sandoghchi, R. Slavik, E. N. Fokoua, S. Bawn, H. Sakr, I. A. Davidson, A. Taranta, J. P. Thomas, M. N. Petrovich, D. J. Richardson, and F. Poletti, "Record low-loss 1.3 dB/km data transmitting antiresonant hollow core fibre," In *2018 European Conference on Optical Communication (ECOC)*, (pp. 1–3). IEEE, (2018).
9. G. Humbert, J. Knight, G. Bouwmans, P. Russell, D. Williams, P. Roberts, and B. Mangan, "Hollow core photonic crystal fibers for beam delivery," *Opt. Express* **12**(8), 1477–1484 (2004).
10. M. R. A. Hassan, F. Yu, W. J. Wadsworth, and J. C. Knight, "Cavity-based mid-IR fiber gas laser pumped by a diode laser," *Optica* **3**(3), 218–221 (2016).
11. M. I. Hasan, N. Akhmediev, A. Mussot, and W. Chang, "Midinfrared pulse generation by pumping in the normaldispersion regime of a gas-filled hollow-core fiber," *Phys. Rev. Appl.* **12**(1), 014050 (2019).
12. M. I. Hasan, N. Akhmediev, and W. Chang, "Mid-infrared supercontinuum generation in supercritical xenon-filled hollow-core negative curvature fibers," *Opt. Lett.* **41**(21), 5122–5125 (2016).
13. F. Benabid and P. J. Roberts, "Linear and nonlinear optical properties of hollow core photonic crystal fiber," *J. Mod. Opt.* **58**(2), 87–124 (2011).
14. X. Zhang, S. Gao, Y. Wang, W. Ding, X. Wang, and P. Wang, "7-cell hollow-core photonic bandgap fiber with broad spectral bandwidth and low loss," *Opt. Express* **27**(8), 11608–11616 (2019).
15. P. Roberts, F. Couny, H. Sabert, B. Mangan, D. Williams, L. Farr, M. Mason, A. Tomlinson, T. Birks, J. Knight, and P. St J Russell, "Ultimate low loss of hollow-core photonic crystal fibres," *Opt. Express* **13**(1), 236–244 (2005).
16. F. Poletti, "Nested antiresonant nodeless hollow core fiber," *Opt. Express* **22**(20), 23807–23828 (2014).
17. W. Belardi, "Design and properties of hollow antiresonant fibers for the visible and near infrared spectral range," *J. Lightwave Technol.* **33**(21), 4497–4503 (2015).
18. F. Yu, W. J. Wadsworth, and J. C. Knight, "Low loss silica hollow core fibers for 3–4 μm spectral region," *Opt. Express* **20**(10), 11153–11158 (2012).
19. M. S. Habib, J. Antonio-Lopez, C. Markos, A. Schülzgen, and R. Amezcua-Correa, "Single-mode, low loss hollow-core anti-resonant fiber designs," *Opt. Express* **27**(4), 3824–3836 (2019).
20. B. Debord, A. Amsanpally, M. Chafer, A. Baz, M. Maurel, J. M. Blondy, E. Hugonnot, F. Scol, L. Vincetti, F. Gérôme, and F. Benabid, "Ultralow transmission loss in inhibited-coupling guiding hollow fibers," *Optica* **4**(2), 209–217 (2017).
21. F. Meng, B. Liu, Y. Li, C. Wang, and M. Hu, "Low loss hollow-core antiresonant fiber with nested elliptical cladding elements," *IEEE Photonics J.* **9**(1), 1–11 (2017).
22. A. Ge, F. Meng, Y. Li, B. Liu, and M. Hu, "Higher-order mode suppression in antiresonant nodeless hollow-core fibers," *Micromachines* **10**(2), 128 (2019).
23. M. I. Hasan, N. Akhmediev, and W. Chang, "Empirical formulae for dispersion and effective mode area in hollow-core antiresonant fibers," *J. Lightwave Technol.* **36**(18), 4060–4065 (2018).

24. Y. Wang, M. I. Hasan, M. R. A. Hassan, and W. Chang, "Effect of the second ring of antiresonant tubes in negative curvature fibers," *Opt. Express* **28**(2), 1168–1176 (2020).
25. X. Chen, X. Hu, L. Yang, J. Peng, H. Li, N. Dai, and J. Li, "Double negative curvature anti-resonance hollow core fiber," *Opt. Express* **27**(14), 19548–19554 (2019).
26. X. Huang, W. Qi, D. Ho, K. T. Yong, F. Luan, and S. Yoo, "Hollow core anti-resonant fiber with split cladding," *Opt. Express* **24**(7), 7670–7678 (2016).
27. M. M. Rahman, A. Khaleque, M. T. Rahman, and F. Rabbi, "Gold-coated photonic crystal fiber-based polarization filter for dual communication windows," *Opt. Commun.* **461**, 125293 (2020).
28. R. T. Schermer and J. H. Cole, "Improved bend loss formula verified for optical fiber by simulation and experiment," *IEEE J. Quantum Electron.* **43**(10), 899–909 (2007).
29. A. Ventura, J. G. Hayashi, J. Cimek, F. B. Slimen, N. White, H. Sakr, N. V. Wheeler, and F. Poletti, "Tellurite antiresonant hollow core microstructured fiber for mid-ir power delivery," *Frontiers in Optics + Laser Science APS/DLS*, OSA Technical Digest (Optical Society of America, 2019) JTU4A–17.
30. A. Cruz, C. Cordeiro, and M. Franco, "3D Printed Hollow-Core Terahertz Fibers," *Fibers* **6**(3), 43 (2018).